Two-dimensional (2+*n*) resonance enhanced multiphoton ionization of HCl: State interactions and photorupture channels via low-energy triplet Rydberg states

Ágúst Kvaran,[a] Kristján Matthiasson, and Huasheng Wang
Science Institute, University of Iceland, Dunhagi 3, 107 Reykjavík, Iceland

(Received 7 May 2009; accepted 25 June 2009; published online 29 July 2009)

Mass spectra were recorded for (2+*n*) resonance enhanced multiphoton ionization (REMPI) of HCl as a function of resonance excitation energy in the 81 710–82 870 cm^{-1} region to obtain two-dimensional REMPI data. Small but significant fragmentations and H^+, Cl^+, as well as HCl^+ formations are found to occur after resonance excitations to the triplet Rydberg states $f\,^3\Delta_2(v'=0)$, $f\,^3\Delta_1(v'=0)$, and $g\,^3\Sigma^+(1)(v'=0)$. Whereas insignificant rotational line shifts could be observed, alterations in relative ion signal intensities, due to perturbations, clearly could be seen, making such data ideal for detecting and analyzing weak state interactions. Model analysis of relative ion signal intensities, taking account of the major ion formation channels following excitations to Rydberg states, its near-resonance interactions with ion-pair states as well as dissociations and/or photodissociations were performed. These allowed verification of the existence of all these major channels as well as quantifications of the relative weights of the channels and estimates of state interaction strengths. The proposed mechanisms were supported by ion signal power dependence studies. © *2009 American Institute of Physics*. [DOI: 10.1063/1.3180824]

I. INTRODUCTION

Since the original work by Price[1] on hydrogen halides, a wealth of spectroscopic data on HCl has been derived from absorption spectroscopy,[2–5] fluorescence studies,[5] as well as resonance enhanced multiphoton ionization (REMPI) experiments.[6–15] Relatively intense single- and multiphoton absorptions in conjunction with electron excitations as well as rich band structured spectra make the molecule ideal for fundamental studies. A large number of Rydberg states, several low-lying repulsive states as well as the $V(^1\Sigma^+)$ ion-pair state have been identified. A number of spin-forbidden transitions have been observed, indicating that spin-orbit coupling is important in excited states of the molecule. Perturbations due to state mixing are widely seen both in absorption[3–5] and REMPI spectra.[7,8,10–12,15] The perturbations appear either as line shifts[4,7,8,11,12,15] or as intensity and/or bandwidth alterations.[4,7,8,10–12,15] Pronounced ion-pair to Rydberg state mixings are both observed experimentally[3,4,8,11,12,15,16] and predicted from theory.[16,17] Interactions between the $V(^1\Sigma^+)$ ion-pair state and the $E(^1\Sigma^+)$ state are found to be particularly strong and to exhibit nontrivial rotational, vibrational, and electron spectroscopy. Perturbations due to Rydberg–Rydberg mixings have also been predicted and identified.[4,10] Both homogeneous ($\Delta\Omega=0$) (Refs. 11, 12, 16, and 17) and heterogeneous ($\Delta\Omega>0$) (Refs. 12, 15, and 16) couplings have been reported. Such quantitative data on molecule-photon interactions are of interest in understanding stratospheric photochemistry as well as being relevant to the photochemistry of planetary atmospheres and the interstellar medium.[5]

Photorupture studies of HCl have revealed a large variety of photodissociation and photoionization processes. In a detailed two-photon REMPI study, Green *et al.*[7] reported HCl^+, Cl^+, and H^+ ion formations for excitations via large number of $\Omega=0$ Rydberg states as well as via the $V\,^1\Sigma^+(\Omega=0)$ ion-pair state, whereas excitations via other Rydberg states were mostly found to yield HCl^+ ions. More detailed investigations of excitations via various Rydberg states and the $V\,^1\Sigma^+$ ion-pair state using photofragment imaging and/or mass-resolved REMPI techniques have revealed several ionization channels depending on the nature of the resonance excited state.[18–22] Results are largely based on analysis of excitations via the $E\,^1\Sigma^+$ Rydberg state and the $V\,^1\Sigma^+$ ion-pair state, which couple strongly to produce the mixed (adiabatic) $B\,^1\Sigma^+$ state with two minima. Also, analysis of excitations via the $F\,^1\Delta_2(v'=1)$ Rydberg state and the $V\,^1\Sigma^+(v'=14)$ state has shown the characteristic effects of near-resonance interactions on photoionization channels.[22] Analysis of excitations via triplet states, however, has not revealed fragmentations or shown the effects of coupling with the ion-pair state.[7,20] These studies reveal characteristic ionization channels that have been summarized in terms of excitations via (1) resonance noncoupled (diabatic) Rydberg state excitations and (2) resonance noncoupled ion-pair excitations.[22] The major channels are as follows:

(1) An ionization via a noncoupled Rydberg state is found to involve (i) one-photon ionization of the Rydberg states to form the molecular ion HCl^+, followed by (ii) a second one-photon excitation to a repulsive ion state ($(2)^2\Pi$) and dissociation to form H^+ (see Fig. 1). HCl^+ could be formed partly by direct ionization and partly by autoionization.[19]
(2) Several ionization channels, via the noncoupled ion-

[a]Author to whom correspondence should be addressed, Telephone: +354-525-4694 and +354-525-4800. Fax: +354-552-8911. Electronic mail: agust@hi.is. URL: http://www.hi.is/~agust/.

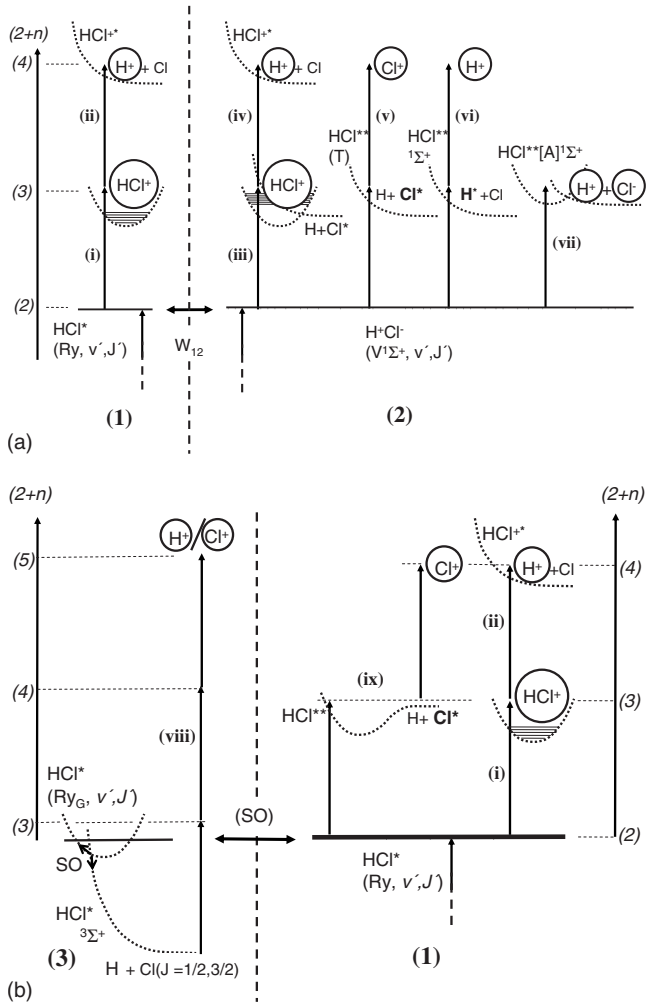

FIG. 1. Ionization mechanisms. Schematics (a) and (b) showing possible ionization channels following excitations and/or state transfer (1) to a diabatic Rydberg state [channels (i), (ii), and (ix)], (2) to a hypothetical diabatic $V\,^1\Sigma^+$ ion-pair state [channels (iii)–(vii)], and (3) to neutral fragments ($H+Cl(^2P_{1/2,3/2})$) via predissociation of a gateway Rydberg state (viii). The arrows represent excitations relevant to $(2+n;n=1-3)$ REMPI. Fragments and excited state species are indicated. The ions formed are highlighted with circles. The total number of photons is indicated.

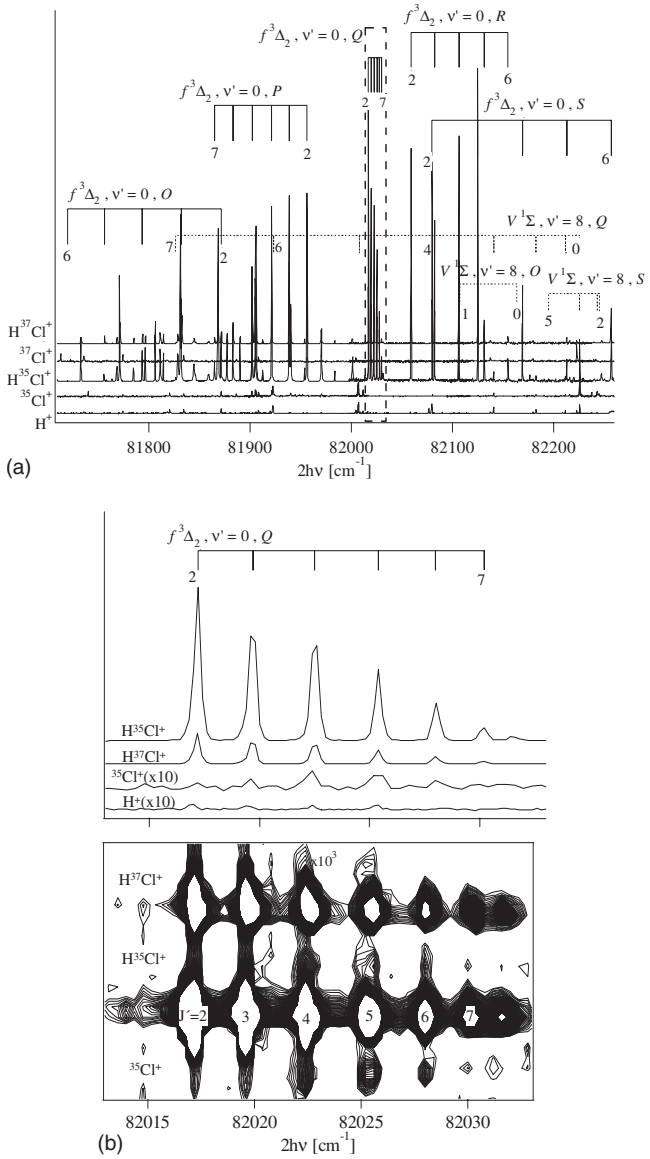

FIG. 2. (a) 1D $(2+n)$ REMPI spectra for H^+, $^{35}Cl^+$, $H^{35}Cl^+$, $^{37}Cl^+$, and $H^{37}Cl^+$ derived from HCl with isotope ratios in natural abundance for the two-photon excitation region of 81 710–82 260 cm^{-1}. Assignments for the $f\,^3\Delta_2 \leftarrow\leftarrow X\,^1\Sigma^+$, (0,0), O,P,Q,R,S line and $V\,^1\Sigma^+ \leftarrow\leftarrow X\,^1\Sigma^+$, (8,0), O,Q,S line transitions are shown. (b) 2D $(2+n)$ REMPI contour (below) for chlorine-containing ions and 1D $(2+n)$ REMPI spectra (above) for H^+, $^{35}Cl^+$, $H^{37}Cl^+$, and $H^{35}Cl^+$ derived from HCl with isotope ratios in natural abundance for the two-photon excitation region of 82 013–82 033 cm^{-1}. Assignments for the $f\,^3\Delta_2 \leftarrow\leftarrow X\,^1\Sigma^+$, (0,0), Q line transitions are shown. $J=J'$-numbers are indicated in the figures.

pair state, have been proposed,[18–21] involving (iii) one-photon autoionization via a repulsive superexcited state that correlates with $H+Cl^*$ to form HCl^+ largely in high vibrational (v^+) levels,[19] followed by (iv) a second one-photon excitation to a repulsive ion state ($(2)^2\Pi$) and dissociation [analogous to (ii)], (v) one-photon excitation to repulsive triplet superexcited states,[20,21] forming H and $Cl^*(Cl^*=Cl^*(4s,4p,3d))$, followed by one-photon ionization of Cl^* to form Cl^+, (vi) one-photon excitation to a repulsive superexcited state (HCl^*, $^1\Sigma^+$), forming $H^*(n=2)$ and Cl, followed by one-photon ionization of $H^*(n=2)$ to form H^+, and (vii) one-photon excitation to a bound superexcited state, which acts as a gateway state to dissociation into the ion-pair H^++Cl^-.[18] More channels have been proposed[18,20] via the "noncoupled" ion-pair state but these are believed to be of minor importance.

Thus, based on this overall ionization scheme H^+ formation clearly is indicative of both the ion-pair and the Rydberg state contribution, whereas the Cl^+ ions are characteristic indicators for the ion-pair state contribution. There are reasons to believe that the HCl^+ contribution to ion formation, via excitation to the V state, is rather small.[22] Therefore HCl^+ formation is the main ion formation channel via Rydberg state excitation [channel (i)] under low power conditions. Therefore, working with relative (normalized) ion intensities for Cl^+ ($I(Cl^+)/I(HCl^+)$) and for HCl^+ ($I(HCl^+)/I(Cl^+)$) as indicators for the separate (diabatic) Rydberg and ion-pair states, respectively, has been found to be useful.

In addition to the photorupture channels mentioned above, further dissociation and/or photodissociation of reso-

nance excited Rydberg states could occur. Thus dissociations to form $H+Cl(J=1/2,3/2)$ via predissociation of some gateway states could be important, as predicted by Alexander *et al.*[23] In such cases, further photoionization of the $Cl(J=1/2,3/2)$ and H fragments could also occur [see channel (viii) in Fig. 1(b)]. Whereas the interactions between the states involved could be of various kinds,[23] spin-orbit couplings most probably are dominant. Alternatively, dissociations via photoexcitations to inner walls of bound (super-)excited Rydberg states above dissociation limits could form $H+Cl^*$ and/or H^*+Cl [see channel (ix) in Fig. 1(b)]. We call channels (viii) and (ix) the "dissociation channels" hereafter.

In this paper, we use a two-dimensional (2D) REMPI approach, obtained by recording ion mass spectra as a function of the laser frequency, to study the photorupture dynamics of HCl for two-photon resonance excitations via the triplet Rydberg states $f\,^3\Delta_2(v'=0)$, $f\,^3\Delta_1(v'=0)$ and $g\,^3\Sigma^+(1)(v'=0)$ and the $V\,^1\Sigma^+(v'=8,9)$ ion-pair states. We show, for the first time, that small but significant fragmentations and H^+ and Cl^+ formations occur after resonance excitations to the triplet states. Whereas insignificant line shifts are seen, rotational quantum-level-dependent ion signal intensities due to perturbation effects are observed for all the states. Thus, relative signal intensities are found to be more sensitive measures of state interactions than line shifts. This was proved to be a useful tool in assisting with state assignment[24] and could possibly be used for indirect characterization of hidden states. A model, based on the major photorupture channels mentioned above, is created and used to simulate ion signal data for ionizations via excitations to the Rydberg states. Thus, the observations are found to be consistent with (a) near-resonance couplings between the triplet states and $V\,^1\Sigma^+$ states and (b) photodissociation via the dissociation channels. The importance of the dissociation channels is found to be Rydberg state dependent. The model further allows estimates of various interaction and weight parameters relevant to the photorupture mechanism. The proposed mechanisms for resonance diabatic state excitations are supported by ion signal power dependence studies.

II. EXPERIMENTAL

2D REMPI data for jet-cooled HCl gas were recorded. Ions were directed into a time-of-flight tube and detected by a microchannel plate (MCP) detector to record the ion yield as a function of mass and laser radiation wavenumber.

The apparatus used is similar to that described elsewhere.[14,25] Tunable excitation radiation in the 241.2–245.0 nm wavelength region was generated by excimer laser-pumped dye laser systems, using a Lambda Physik COMPex 205 excimer laser and a Coherent ScanMatePro dye laser. Dye C-480 was used and frequency doubling was obtained with a Beta Barium Borate-2 (BBO-2) crystal. The repetition rate was typically 10 Hz. The bandwidth of the dye laser beam was about 0.095 cm^{-1}. The typical laser intensity used was 0.1–0.3 mJ/pulse. The radiation was focused into an ionization chamber between a repeller and an extractor plate. We operated the jet in conditions that limited cooling in order not to lose the transitions from the high rotational levels. Thus, an undiluted, pure HCl gas sample (Merck-Schuchardt OHG; purity >99.5%) was used. It was pumped through a 500 μm pulsed nozzle from a typical total backing pressure of about 1.0–1.5 bars into the ionization chamber. The pressure in the ionization chamber was lower than 10^{-6} mbar during experiments. The nozzle was kept open for about 200 μs, and the laser beam was typically fired 500 μs after the nozzle was opened. Ions were extracted into a time-of-flight tube and focused on a MCP detector, of which the signal was fed into a LeCroy 9310A, 400 MHz storage oscilloscope, as a function of the flight time. The average signal levels were evaluated and recorded for a fixed number of laser pulses (typically 100 pulses) to obtain the mass spectra. Mass spectra were typically recorded in 0.05 or 0.1 cm^{-1} laser wavenumber steps to obtain 2D REMPI spectra. REMPI spectra for certain ions as a function of excitation wavenumber [one-dimensional (1D) REMPI] were obtained by integrating signal intensities for narrow time-of-flight (hence, mass) ranges covering the particular ion mass. The power dependence of the ion signal was determined by integrating the mass signals repeatedly and averaging for ~1000 pulses, after bypassing a different number of quartz windows to reduce power. Care was taken to prevent saturation effects as well as power broadening by minimizing laser power. La-

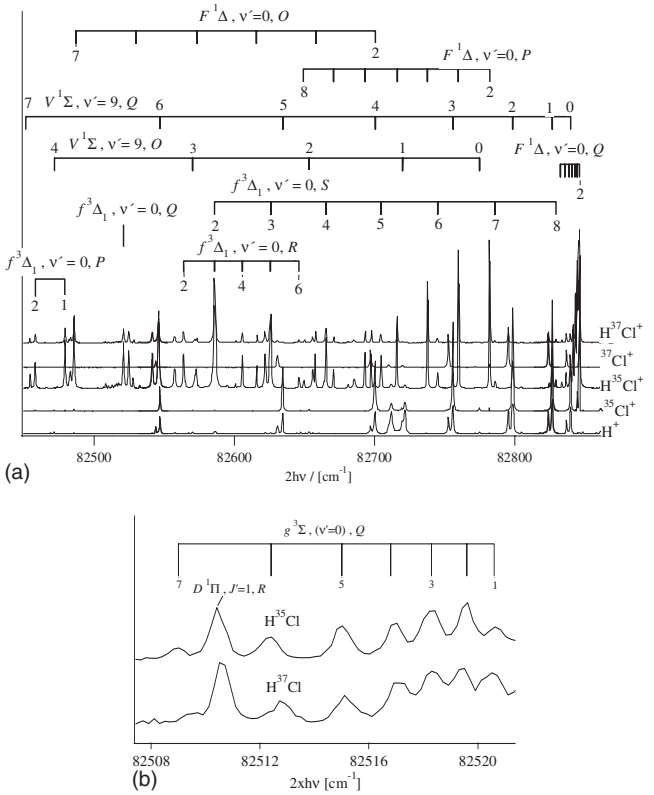

FIG. 3. (a) 1D $(2+n)$ REMPI spectra for H^+, $^{35}Cl^+$, $H^{35}Cl^+$, $^{37}Cl^+$, and $H^{37}Cl^+$ derived from HCl with isotope ratios in natural abundance for the two-photon excitation region of 82 450–82 870 cm^{-1}. Assignments for the $f\,^3\Delta_1 \leftarrow\leftarrow X\,^1\Sigma^+$, (0,0), P,Q,R,S line and $V\,^1\Sigma^+ \leftarrow\leftarrow X\,^1\Sigma^+$, (9,0), O,Q line and $F\,^1\Delta_2 \leftarrow\leftarrow X\,^1\Sigma^+$ (0,0), O,P,Q line transitions are shown. (b) 1D $(2+n)$ REMPI spectra for $H^{35}Cl^+$ and $H^{37}Cl^+$ for the region of 82 508–82 522 cm^{-1}. Assignments for the $g\,^3\Sigma^+(1) \leftarrow\leftarrow X\,^1\Sigma^+$, (0,0), Q line and the $D\,^1\Pi_1 \leftarrow\leftarrow X\,^1\Sigma^+$, (0,0), R, $J'=1$ line transitions are shown. $J=J'$-numbers are indicated in the figures.

TABLE I. Rotational lines of relevant transitions derived by Green *et al.* (Ref. 9) (marked "others") and us ("ours") (cm^{-1}). The accuracy of "our" values is about ± 1.0 cm^{-1}.

	$f\,^3\Delta_2 \leftarrow\leftarrow X\,^1\Sigma^+(0,0)$									
	O		P		Q		R		S	
J'	Others	Ours	Others	Ours	Others	Ours	Others	Ours	Others	Ours
2	81 871.3	81 871.8	81 954.5	81 956.4	82 017.2	82 017.2	82 059.3	82 059.3	82 080.0	82 079.9
3		81 832.4	81 936.8	81 938.8	82 019.8	82 019.7	82 082.7	82 082.4	82 124.1	82 125.1
4	81 793.6	81 793.5	81 919.0	81 921.6	82 022.9	82 022.5	82 106.0	82 106.3	82 168.4	82 169.2
5	81 754.8	81 756.2	81 900.9	81 902.3	82 025.6	82 025.4	82 129.8	82 131.1	82 212.7	82 212.9
6		81 719.8	81 883.1	81 883.4		82 028.0		82 154.7	82 256.8	82256.5
7			81 865.0	81 864.9		82 030.2				

	$f\,^3\Delta_1 \leftarrow\leftarrow X\,^1\Sigma^+(0,0)$								$g\,^3\Sigma^+(1) \leftarrow\leftarrow X\,^1\Sigma^+(0,0)$
	P		Q		R		S		Q
J'	Others	Ours	Others	Ours	Others	Ours	Others	Ours	Ours
1	82 481.4	82 478.9	82 523.2	82 521.0					82 520.8
2	82 460.0	82 458.1			82 564.8	82 563.8	82 585.6	82 585.8	82 519.7
3					82 584.7	82 585.8	82 626.4	82 626.1	82 518.5
4					82 605.0	82 605.7	82 666.9	82 665.4	82 517.2
5						82 625.9	82 707.3	82 704.8	82 515.3
6					82 645.4	82 646.2	82 748.0	82 745.0	82 512.8
7							82 788.1	82 786.0	82 509.4
8									82 504.4

	$V\,^1\Sigma^+ \leftarrow\leftarrow X\,^1\Sigma^+(8,0)$						$V\,^1\Sigma^+ \leftarrow\leftarrow X\,^1\Sigma^+(9,0)$				
	O		Q		S		O		Q		S
J'	Others	Ours	Others	Ours	Others	Ours	Others	Ours	Others	Ours	Others
0	82 163.3		82 225.7	82 225.7			82 777.0	82 774.7	82 839.7	82 839.7	82 862.0
1	82 106.9	82 107.5	82 211.3	82 211.7			82 721.8	82 721.8	82 826.3	82 826.7	82 862.6
2			82 182.0	82 182.6	82 244.8	82 244.9	82 653.2	82 653.8	82 799.2	82 798.6	
3			82 140.3	82 140.7	82 242.8	82 242.9		82 570.0	82 758.1	82 755.8	
4				82 080.3		82 225.7		82 471.5	82 703.1	82 700.3	
5				82 007.8	82 194.9	82 194.8				82 634.5	
6				81 923.6		82 244.9				82 547.0	
7				81 826.8		82 242.9				82 451.4	

ser calibration was performed by recording an optogalvanic spectrum, obtained from a built-in neon cell, simultaneously with the recording of the REMPI spectra. The atomic reference lines, for absolute wavelength calibration (5 pm accuracy), were provided using an optical SPOCK (Simulation Program for Optical Circuit Knowledge) function. Line positions were also compared to the strongest hydrogen chloride rotational lines reported by Green *et al.*[9] The accuracy of the calibration was found to be about ± 1.0 cm^{-1} on a two-photon wavenumber scale. Intensity drifts during the scan were taken into account, and spectral intensities were corrected for accordingly.

III. RESULTS AND ANALYSIS

A. Two-dimensional REMPI and relative ion signals

Figure 2(a) shows 1D $(2+n)$ REMPI spectra for H^+, $^{35}Cl^+$, $H^{35}Cl^+$, $^{37}Cl^+$, and $H^{37}Cl^+$ derived from HCl with isotope ratios in natural abundance for the two-photon excitation region of 81 710–82 260 cm^{-1}. Figure 2(b) shows the corresponding 2D REMPI contour (below) and 1D REMPI spectra (above) for the narrow spectral region of 82 013–82 033 cm^{-1}. Figure 3(a) shows the $(2+n)$ REMPI spectra for H^+, $^{35}Cl^+$, $H^{35}Cl^+$, $^{37}Cl^+$, and $H^{37}Cl^+$ for the two-photon excitation region of 82 450–82 870 cm^{-1}. Figure 3(b) shows the expanded $(2+n)$ REMPI spectra for $H^{35}Cl^+$ and $H^{37}Cl^+$ for the region of 82 508–82 522 cm^{-1}. By comparison with data reported by Green *et al.*,[7] rotational peaks due to the transitions $f\,^3\Delta_2 \leftarrow\leftarrow X\,^1\Sigma^+(0,0)$, $f\,^3\Delta_1 \leftarrow\leftarrow X\,^1\Sigma^+(0,0)$, $V\,^1\Sigma^+ \leftarrow\leftarrow X\,^1\Sigma^+(8,0)$, $V\,^1\Sigma^+ \leftarrow\leftarrow X\,^1\Sigma^+(9,0)$, and $F\,^1\Delta_2 \leftarrow\leftarrow X\,^1\Sigma^+(0,0)$ for $H^{35}Cl$ have been identified and assigned. In addition, several more rotational lines have been assigned to these electronic transitions (see also Table I). The major structure in Fig. 3(b) is due to the resonance transition $g\,^3\Sigma^+(1) \leftarrow\leftarrow X\,^1\Sigma^+$.[24] Other peaks observed in this region are due to the transitions $d\,^3\Pi(0^+) \leftarrow\leftarrow X\,^1\Sigma^+$ and $D\,^1\Pi(1) \leftarrow\leftarrow X\,^1\Sigma^+(0,0)$.[7]

On a relative scale, significant ion signals for all ion species are observed for the $V\,^1\Sigma^+ \leftarrow\leftarrow X\,^1\Sigma^+(8,0)$ and $V\,^1\Sigma^+ \leftarrow\leftarrow X\,^1\Sigma^+(9,0)$ systems, whereas the parent ion signals dominate the REMPI for $f\,^3\Delta_2 \leftarrow\leftarrow X\,^1\Sigma^+(0,0)$, $f\,^3\Delta_1 \leftarrow\leftarrow X\,^1\Sigma^+(0,0)$, and $g\,^3\Sigma^+(1) \leftarrow\leftarrow X\,^1\Sigma^+$, in agreement with earlier observations.[7,24] Weak but significant H^+, $^{35}Cl^+$, and $^{37}Cl^+$, however, are also observed for the

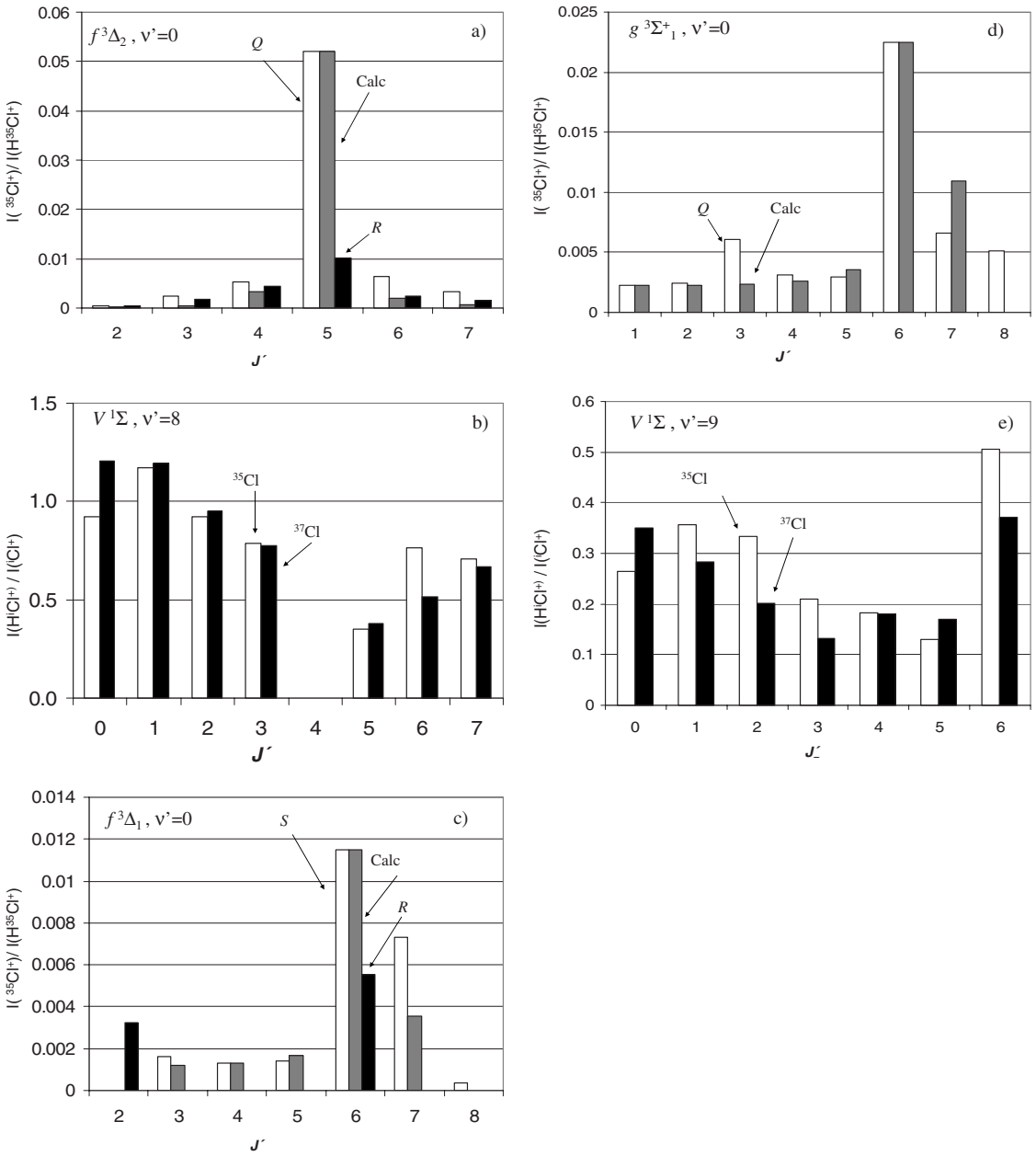

FIG. 4. Relative (normalized) ion signal intensities, (a) $I(^{35}Cl^+)/I(H^{35}Cl^+)$ for $f\ ^3\Delta_2 \leftarrow\leftarrow X\ ^1\Sigma^+$, (0,0), derived from the following: (i) Q rotational lines (white columns), (ii) R lines (black columns), and (iii) simulations of the data for the Q lines, marked as "calc." (gray columns; see text). (b) $I(H^{35}Cl^+)/I(^{35}Cl^+))$ and $(I(H^{37}Cl^+)/I(^{37}Cl^+))$ for $V\ ^1\Sigma^+ \leftarrow\leftarrow X\ ^1\Sigma^+$, (8,0), derived from Q lines. Ratios for $J'=4$ could not be derived because of rotational line overlapping. (c) $I(^{35}Cl^+)/I(H^{35}Cl^+)$ for $f\ ^3\Delta_1 \leftarrow\leftarrow X\ ^1\Sigma^+$, (0,0), derived from the following: (i) S lines (white columns), (ii) R lines (black columns), and (iii) simulations of the data for the S lines, marked as calc. (gray columns; see text). (d) $I(^{35}Cl^+)/I(H^{35}Cl^+)$ for $g\ ^3\Sigma^+(1) \leftarrow\leftarrow X\ ^1\Sigma^+$, (0,0), derived from the following: (i) Q lines (white columns), (ii) simulations of the data for the Q lines, marked as calc. (gray columns; see text). (e) $I(H^{35}Cl^+)/I(^{35}Cl^+))$ and $(I(H^{37}Cl^+)/I(^{37}Cl^+)$ for $V\ ^1\Sigma^+ \leftarrow\leftarrow X\ ^1\Sigma^+$, (9,0), derived from Q lines.

transitions to the triplet states. The observation for the $V\ ^1\Sigma^+ \leftarrow\leftarrow X\ ^1\Sigma^+$, (8,0) and (9,0) systems is in agreement with earlier observations[7,22] and expectations.[22] Relative (normalized) ion signal intensities for the systems of concern are shown in Fig. 4.

Weak but significant enhancement of the normalized $^{35}Cl^+$ signal intensity is observed for $f\ ^3\Delta_2 \leftarrow\leftarrow X\ ^1\Sigma^+$, (0,0), Q line, $J'=5$ [see Fig. 4(a)]. This corresponds to the smallest spacing between the rotational energy levels in the $f\ ^3\Delta_2(v'=0)$ and the $V\ ^1\Sigma^+(v'=8)$ states for the same $J'=5$ value (see Table II), suggesting a near-resonance interaction between the two states.[12,15,22] This effect does not show as an enhanced normalized $H^{35}Cl^+$ signal for the $V\ ^1\Sigma^+ \leftarrow\leftarrow X\ ^1\Sigma^+$, (8,0) system [see Fig. 4(b)], however, underlining the interaction weakness. No significant shifts of rotational energy levels or irregularities in line spacing could be seen for either of these two systems, further underlining the interaction weakness. Weak but significant enhancement of the normalized $^{35}Cl^+$ signal intensity is observed for both systems $f\ ^3\Delta_1 \leftarrow\leftarrow X\ ^1\Sigma^+$, (0,0), S line and $g\ ^3\Sigma^+(1) \leftarrow\leftarrow X\ ^1\Sigma^+(0,0)$, Q line for $J'=6$. This also corresponds to the smallest spacing between the rotational energy levels in the Rydberg states and the closest ion-pair state, $V\ ^1\Sigma^+(v'=9)$ for the same $J'=6$ value (see Table II), also

TABLE II. $\Delta E_{J'}$ relevant to near-resonance interactions for $f\,^3\Delta_2 \leftrightarrow V\,^1\Sigma^+$, $v'=8$, $f\,^3\Delta_1 \leftrightarrow V\,^1\Sigma^+$, $v'=9$, and $g\,^3\Sigma^+(1) \leftrightarrow V\,^1\Sigma^+$, $v'=9$.

J'	$\Delta E=E(f\,^3\Delta_2;v'=0)-E(V\,^1\Sigma^+;v'=8)$ (cm^{-1})	$\Delta E=E(f\,^3\Delta_1;v'=0)-E(V\,^1\Sigma^+;v'=9)$ (cm^{-1})	$\Delta E=E(g\,^3\Sigma^+(1);v'=0)-E(V\,^1\Sigma^+;v'=9)$ (cm^{-1})
1		−303.0	−305.4
2	−164.9	−276.2	−279.5
3	−119.9	−235.9	−239.4
4	−57.49	−180.8	−184.6
5	17.7	−113.7	−118.2
6	105.4	−27.9	−34.2
7	203.4	66.5	57.9

indicating near-resonance interactions. Close to constant, nonzero "background values" are obtained for other J's which we believe correspond to the existence of the dissociation channels (see below). Now an enhanced normalized $H^{35}Cl^+$ signal for the $V\,^1\Sigma^+ \leftarrow\leftarrow X\,^1\Sigma^+(9,0)$ system, $J'=6$, is clearly observed, whereas no significant shifts of rotational energy levels or irregularities in line spacing could be seen for any of these systems. The overall trends in relative signal strengths observed for the $V\,^1\Sigma^+ \leftarrow\leftarrow X\,^1\Sigma^+(8,0)$ and (9,0) systems [Figs. 4(b) and 4(e)] are due to nonresonance interactions between these states and other singlet Rydberg states. Thus, significant drops in the signal strengths observed for $V\,^1\Sigma^+ \leftarrow\leftarrow X\,^1\Sigma^+(8,0)$, $1 \le J' \le 5$ and for $V\,^1\Sigma^+ \leftarrow\leftarrow X\,^1\Sigma^+(9,0)$, $0 \le J' \le 5$ could largely be due to decreasing interactions with the singlet Rydberg state $E\,^1\Sigma^+(v'=0)$ and $D\,^1\Pi(v'=0)$ in the former case and decreasing interactions with $E\,^1\Sigma^+(v'=0)$ in the latter case.[11,12,16,22] Analogous but less clear effects were also seen for normalized H^+ signal intensities.

B. State interactions versus excitation mechanisms

Assuming a level-to-level interaction scheme holds for Rydberg (**1**) to ion-pair (**2**) state interactions (Fig. 1), weight factors (fractions) for the state mixing can be expressed as follows:

$$c_i^2 = \frac{1}{2} \pm \frac{\sqrt{|\Delta E|^2 - 4|W_{12}|^2}}{2|\Delta E|}, \tag{1}$$

for $\Delta E = E_1 - E_2$, where E_1 and E_2 are the resulting level energies of the perturbed states (**1**) and (**2**) and W_{12} is the matrix element of the perturbation function/interaction strength.[22,26] In the case of homogeneous ($\Delta\Omega=0$) interaction, W_{12} is independent of the total angular momentum quantum number, J', whereas for heterogeneous ($\Delta\Omega>0$) interactions W_{12} is expressed as follows:[12,22,27]

$$W_{12} = W'_{12}(J'(J'+1))^{1/2}, \tag{2}$$

for constant W'_{12}. W_{12} is related to the resulting level energies and the zero-order level energies for the unperturbed state (E_1^0 and E_2^0; $\Delta E^0 = E_1^0 - E_2^0$) by the following:

$$E_i = \tfrac{1}{2}(E_1^0 + E_2^0) \pm \tfrac{1}{2}[4|W_{12}|^2 + (\Delta E^0)^2]^{1/2}. \tag{3}$$

Assuming the mechanism, discussed before [see Fig. 1; channels (i)–(ix)], holds, we make the following assumptions: The Cl^+ ion intensity observed ($I(Cl^+)$) is proportional to the fraction of HCl^* in the ion-pair state [(**2**); c_2^2] as well as its fraction in the Rydberg state [(**1**); c_1^2],

$$I(Cl^+) = \alpha_2 c_2^2 + \beta_1 c_1^2. \tag{4}$$

Similarly, the HCl^+ intensity ($I(HCl^+)$) is assumed to be proportional to the same fractions,

$$I(HCl^+) = \alpha_1 c_1^2 + \beta_2 c_2^2. \tag{5}$$

For $\alpha = \alpha_2/\alpha_1$, $\gamma = \beta_1/\alpha_2$, $\delta = 1-(\beta_2/\alpha_1)$, and $c_1^2 = 1 - c_2^2$, the ratio of $I(Cl^+)$ over $I(HCl^+)$ now can be expressed as

$$\frac{I(Cl^+)}{I(HCl^+)} = \alpha \frac{(\gamma + c_2^2(1-\gamma))}{(1-\delta c_2^2)}. \tag{6}$$

There is reason to believe that the contribution to the HCl^+ formation [see Eq. (5)] by excitation from the diabatic ion-pair state is small;[22] hence, the ratio of the proportionality factor (β_2) to that for the HCl^+ formation from the diabatic Rydberg state, α_1 (i.e., β_2/α_1), is negligible and $\delta \sim 1$. By combining Eqs. (1), (2), and (6) and assuming $\delta=1$, the following expression is derived:

$$\frac{I(Cl^+)}{I(HCl^+)} = \frac{\alpha\left[\gamma + \left\{\frac{1}{2} - \frac{\sqrt{|\Delta E(J')|^2 - 4W_{12}'^2 J'(J'+1)}}{2|\Delta E(J')|}\right\}(1-\gamma)\right]}{1 - \left[\frac{1}{2} - \frac{\sqrt{|\Delta E(J')|^2 - 4W_{12}'^2 J'(J'+1)}}{2|\Delta E(J')|}\right]}, \tag{7}$$

TABLE III. Parameter values in the least square fit model for ion intensity ratios ($I(Cl^+)/I(HCl^+)$) as a function of J'; see Eq. (7), related equations, and discussion Sec. III B.

	$f\,^3\Delta_2;\ v'=0$	$f\,^3\Delta_1;\ v'=0$	$g\,^3\Sigma^+(1)$
J' near resonance (J'_{res})	5	6	6
$\Delta(\Delta E)_{max}/cm^{-1}$ [a,b]	0.5	1.0	2.0
W_{12}^{max} ($c^2_{1,min}$) [a–c]	2	4	6
$c^2_{1,min}$ [a,c]	0.987	0.979	0.968
W'^{max}_{12}/cm^{-1} [a,d]	0.4	0.7	1.0
$\gamma\ (=\beta_1/\alpha_2)$	0	0.002	0.004
$\alpha\ (=\alpha_2/\alpha_1)$	4.0	0.5	0.6

[a]See text.
[b]See Eq. (8).
[c]See Eq. (1).
[d]See Eq. (2).

for excitations via Rydberg (**1**) state. This expression allows relative ion signal data, such as that shown in Figs. 4(a), 4(c), and 4(d), to be fitted for known ΔE values (see Table II) using the variables γ, α, and W'_{12}. These three parameters now will be discussed in more detail.

$\gamma\ (=\beta_1/\alpha_2)$ is a measure of the rate of formation of Cl^+ via the diabatic Rydberg state (the dissociation channels) to that of its formation from the diabatic ion-pair state. The latter Cl^+ formation process is one of the major (characteristic) ionization channels. Hence γ is a relative measure of the importance of the dissociation channels.

$\alpha\ (=\alpha_2/\alpha_1)$ measures the relative rate of the two major/characteristic ionization channels, i.e., for the Cl^+ formation for excitation from the diabatic ion-pair state (α_2) to the HCl^+ formation from the diabatic Rydberg state (α_1). Considering the fact that the Cl^+ ion signals via excitations to the ion-pair states and the HCl^+ ion signals via excitations to the Rydberg states are comparable or of the same order of magnitude (see Figs. 2 and 3) we feel that α should be somewhat close to unity and certainly in the range of $10^{-1}<\alpha<10$.

From Eq. (3), W_{12} can be expressed in terms of ΔE and the difference, $\Delta E-\Delta E^0$ ($=\Delta(\Delta E)$), as

$$|W_{12}| = \tfrac{1}{2}\sqrt{(\Delta E)^2 - (\Delta E - \Delta(\Delta E))^2}. \quad (8)$$

For strong enough near-resonance interactions to show the clear shifts of the rotational peaks, hence, the clear shifts of rotational levels $\Delta(\Delta E)$ and W_{12} can be evaluated.[12,15] Since the interactions here are too weak to show as line/level shifts (see discussion above), only the upper limits for $\Delta(\Delta E)$ [i.e., $\Delta(\Delta E)_{max}$] based on variations in the line/level spacing can be estimated. From these, the upper limit values for W_{12} for the near-resonance rotational levels (J'_{res}) ($W_{12}^{max}(J'_{res})$) and the W'_{12} parameters (W'^{max}_{12}) can be evaluated from Eqs. (8) and (2). These are listed in Table III for the three Rydberg states of concern along with corresponding weight (fraction) factors, c_1^2, which represent the minimum values ($c^2_{1,min}$) derived from Eq. (1). Low W_{12}^{max} (W'^{max}_{12}) and high (i.e., close to unity) $c^2_{1,min}$ values are indicative of small, yet measurable, interaction strengths. By using $W'_{12}=W'^{max}_{12}$ and performing a least square fit of the expression on the right side of Eq. (7) to the data for $I(^{35}Cl^+)/I(H^{35}Cl^+)$ shown in Figs. 4(a), 4(c), and 4(d), the γ and α values listed in Table III were derived. The corresponding calculated (fitted) ion ratios are shown in the same figures (gray columns).

Reasonably good overall fits of calculated to experimental ion ratios ($I(^{35}Cl^+)/I(H^{35}Cl^+)$) versus J' are obtained for all the Rydberg resonance systems analyzed [see Figs. 4(a), 4(c), and 4(d)]. Thus, clear main peaks, corresponding to the resonance interactions, are reproduced in all cases. Slight, but significant, enhancements of the ratios closest to the resonance peaks also are reproduced qualitatively, and in the case of the systems $f\,^3\Delta_1 \leftarrow\leftarrow X\,^1\Sigma^+$, (0,0), S lines and $g\,^3\Sigma^+(1) \leftarrow\leftarrow X\,^1\Sigma^+$, (0,0), Q lines, close to constant, nonzero background values are obtained for other J's corresponding to the existence of the dissociation channels. All in all, this supports the validity of the model as described above and based on the major ionization channels for Cl^+ and HCl^+ formations shown in Fig. 1. Whereas, negligible contribution to the Cl^+ ion formation is found to be from the dissociation channels for resonance excitation to $f\,^3\Delta_2$ ($\gamma=0$; Table III), the increasing weight of its contribution is found for the other triplet Rydberg states as $f\,^3\Delta_1 < g\,^3\Sigma^+(1)$ ($\gamma=0.002$ and 0.004, respectively). This fits with the prediction given by Alexander *et al.*,[23] who showed no spin-orbit coupling between the $f\,^3\Delta_2$ state and the nearby Rydberg state, which could act as a gateway for further predissociation via spin-orbit coupling with a repulsive $t\,^3\Sigma^+$ state, whereas the Rydberg states $C,D\,^1\Pi$ and $b,d\,^3\Pi_1$ all could act as such both for $f\,^3\Delta_1$ and $g\,^3\Sigma^+(1)$. In addition, the nearby $g\,^3\Sigma^-(1)$ Rydberg state could also act as a gateway state for $g\,^3\Sigma^+(1)$ toward predissociation, which might explain the still greater importance of that mechanism for $g\,^3\Sigma^+(1)$.

The small but reproducible enhancement in the $I(^{35}Cl^+)/I(H^{35}Cl^+)$ ratio observed for the $g\,^3\Sigma^+(1) \leftarrow\leftarrow X\,^1\Sigma^+$, (0,0) system, $J'=3$, could not be explained as being due to near-resonance interaction between the $g\,^3\Sigma^+(1)$ state and any neighbor Rydberg or ion-pair state. A possible explanation is the following. Predissociation on repulsive potential energy surfaces for $t\,^3\Sigma^+$ states, via gateway Rydberg states [$C,D\,^1\Pi$, $b,d\,^3\Pi_1$, and $g\,^3\Sigma^-(1)$], will produce $H+Cl(3p,^2P_{3/2})$ and $H+Cl(3p,^2P_{1/2})$ followed by excitations to form $Cl^+ + e^-$. Resonance excitation for the transitions $g\,^3\Sigma^+(1) \leftarrow\leftarrow X\,^1\Sigma^+$, (0,0), Q lines (i.e., two-photon excitations in the region of 82 508–82 522 cm^{-1}) happens to be near resonance with the two-photon transition $Cl^*(4p,^4P_{1/2}) \leftarrow\leftarrow Cl(3p,^2P_{1/2})$ (82 482.58 cm^{-1}),[28] which, although spin forbidden, is allowed in terms of the orbital angular momentum quantum numbers, $l(\Delta l=0)$ and $L(\Delta L=0)$, as well as in terms of the total angular momentum quantum number $J(\Delta J=0)$ with relatively strong transition probability. Therefore, J'-dependent Cl^+ ion formation (over HCl^+ formation) following dissociation by the dissociation channel (viii) [Fig. 1(b)], as seen near $J'=3$ [Fig. 4(d)], could be due to the effects of near-resonance excitations between surfaces correlating with $H+Cl^*(4p,^4P_{1/2})$ and $H+Cl(3p,^2P_{1/2})$ during the dissociation process.

In addition to the ion-ratio values for the $f\,^3\Delta_2 \leftarrow\leftarrow X\,^1\Sigma^+$, (0,0), Q lines and the $f\,^3\Delta_1 \leftarrow\leftarrow X\,^1\Sigma^+$, (0,0), S lines, mentioned above, values derived for the same systems but for R lines were derived [see Figs. 4(a) and 4(c)]. These are consistently found to be lower. In particular, this is the case for the resonance peaks ($J'=5$ for $f\,^3\Delta_2 \leftarrow\leftarrow X\,^1\Sigma^+$, (0,0) [Fig. 4(a)] and $J'=6$ for $f\,^3\Delta_1$

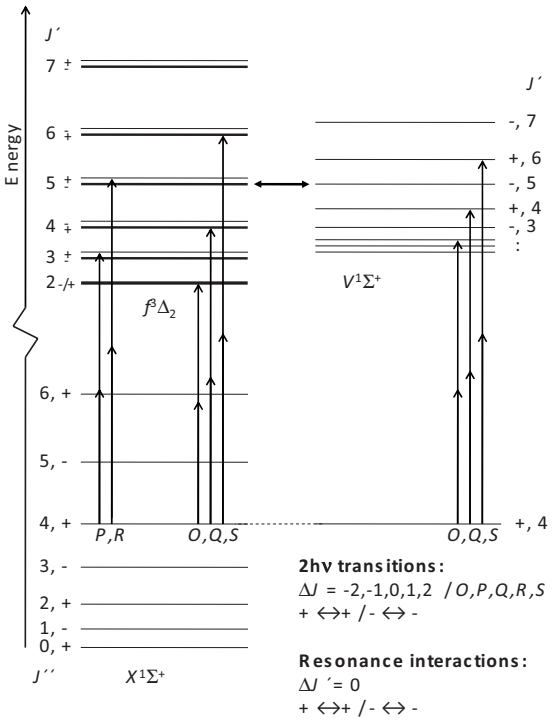

FIG. 5. Schematic energy levels marked with parities (±) and relevant J quantum numbers and selected two-photon transitions ($J''=4$) for the $f\,^3\Delta_2 \leftarrow\leftarrow X\,^1\Sigma^+$ and $V\,^1\Sigma^+ \leftarrow\leftarrow X\,^1\Sigma^+$ electronic transitions and the P,R and O,Q,S rotational transitions. Selection rules relevant to two-photon transitions and state interactions are indicated at the bottom right corner of the figure. According to the selection rules, only the $f(A'')$ state component of the $f\,^3\Delta_2$ state is accessed by the P and R rotational transitions whereas the $e(A')$ state components of the excited states are accessed by the O, Q, and S transitions. Based on the selection rules for state interactions, only crossing between $e(A')$ states components can occur.

$\leftarrow\leftarrow X\,^1\Sigma^+$, (0,0) [Fig. 4(c)]). This can be explained with reference to Fig. 5. Figure 5 shows examples of observable ("allowed") two-photon resonance transitions from the ground state ($X\,^1\Sigma^+$, $J''=4$ used as a particular example) to a Rydberg state [$f\,^3\Delta_2$; $J'=3(P)$, $5(R)$ and $J'=2(O)$, $4(Q)$, $6(S)$] as well as to the ion-pair state [$V\,^1\Sigma^+$; $J'=2(O)$, $4(Q)$, $6(S)$]. Parities of levels (states) are indicated as ±. Observed transitions are determined by the two-photon absorption selection rules,[13,29]

$$+ \leftrightarrow + \quad \text{or} \quad - \leftrightarrow -,$$

$$\Delta J = 0, \pm 1, \pm 2.$$

Thus, the $e(A')$ component of the Rydberg state is accessed by the O, Q, and S lines whereas the $f(A'')$ component is accessed by the P and R lines.[7] Notice that the ground and the ion-pair states consist only of $e(A')$ state components. State interactions between the Rydberg state ($f\,^3\Delta_2$; the same holds for $f\,^3\Delta_1$) and the ion-pair state ($V\,^1\Sigma^+$) are determined by the selection rules,[26]

$$+ \leftrightarrow + \quad \text{or} \quad - \leftrightarrow -,$$

$$\Delta J = 0.$$

Therefore, strictly, only interactions between the $e(A')$ states accessed by the O, Q, and S lines are allowed. Thus, if Cl^+ formation, following resonance excitation to a Rydberg state, was mainly due to interaction with the ion-pair state but was negligible due to the dissociation channels as is the case for excitation to the $f\,^3\Delta_2$ state (see above), one might indeed expect a large drop in the Cl^+ ion intensities for the P and R lines compared to that for the O, Q, and S lines. The fact that the $I(^{35}Cl^+)/I(H\,^{35}Cl^+)$ ratios for the R lines are nonzero, however, and actually peak for $J'=5$, analogous to that found for the Q lines, suggests some violation of the parity selection rule for the state interaction. The clear drop in the ratio value for $f\,^3\Delta_1 \leftarrow\leftarrow X\,^1\Sigma^+$, (0,0), $J'=6$ by going from the S line to the R line shows an analogous effect. However, the ratios both for $J'=6$ and 2, R lines are larger than that observed for the dissociation channels contributions ($J'=3-5$), according to the S lines, suggesting that the relative enhancement is due to some detailed difference in that mechanism depending on whether the transfer is from the $e(A')$ or the $f(A'')$ Rydberg states components.

C. Laser power dependence versus excitation mechanisms

Slope evaluations of log-log plots for the H^+ and H^iCl^+ ($i=35$ and/or 37) ion intensities as a function of laser power,[22] derived for various rotational lines, revealed the number of photons needed to create ions 4 and 3, respectively, in the cases of resonance excitations to all systems of concern ($f\,^3\Delta_2$, $v'=0$; $f\,^3\Delta_1$, $v'=0$; $g\,^3\Sigma^+(1)$, $v'=0$; $V\,^1\Sigma^+$, $v'=8$ and 9). This is what is to be expected in cases of the dominant ion product channels discussed earlier and shown in Fig. 1,[22] which further supports the proposed mechanisms. Analogous analysis of the Cl^+ ion intensities reveals less consistent results with slope values ranging between 3 and 4. Thus, the slope values for log-log plots of $^iCl^+$ ($i=35$ and/or 37) versus laser power for resonance excitations to the $V\,^1\Sigma^+$, $v'=8$ and 9 states, various rotational levels, are found to be close to or slightly larger than 3, whereas the corresponding slope values for the $f\,^3\Delta_1$, $v'=0$ state are closer to 4. Judging from the ionization mechanism (see Fig. 1), four photons or more are what might be needed to create Cl^+. Analogous observations of fractional slope values have been seen before for other systems.[22,30] This could be due to saturation effects in one or more excitation steps resulting in values lower than the nominal number of photons. Such effects would be particularly important for channel (viii), in which case large laser fluence is required to perform as many as five photon excitations to create Cl^+ [see Fig. 1(b)]. Resonance or near-resonance multiphoton excitations of Cl^* and/or ($H+Cl(J=1/2,3/2)$), involved, as discussed before, may complicate things still more.

IV. CONCLUSIONS

2D REMPI data for HCl, obtained by recording ion mass spectra as a function of the laser frequency, were recorded for the two-photon resonance excitation regions of 81 710–82 260 and 82 450–82 870 cm^{-1}. The observed spectra cover the rotational structures due to two-photon resonance transitions to the triplet excited states $f\,^3\Delta_2(v'=0)$, $f\,^3\Delta_1$ $(v'=0)$, $g\,^3\Sigma^+(1)(v'=0)$ and to the ion-

pair states, $V\,^1\Sigma^+(v'=8,9)$ among others. For the first time, small but significant Cl^+ and H^+ ion formations could be observed for the triplet states. Relative (normalized) ion signals, suitable for identifying interactions between Rydberg states and ion-pair states,[22,24] showed that near-resonance interactions occur between all the triplet states and the $V\,^1\Sigma^+(v'=8,9)$ states. This could not be seen or quantified by a more standard way of analyzing line shifts[12,15,26,27] due to the interaction weakness, showing that the relative ion intensities are significantly more sensitive measures of perturbation effects. A model, which takes into account the major ion formation channels following excitations to Rydberg states, its near-resonance interactions with ion-pair states as well as dissociation or photodissociation processes (dissociation channels), was created and used to analyze the data of the ion signals as a function of rotational quantum numbers. Qualitative comparison of the model calculations and experimental data verified the existence of the major channels. Least-square simulation analysis allowed quantifications of relative weights of the channels as well as the upper limits of state interaction strengths. The varying weight of the dissociation channels is found to be consistent with the increasing number of spin-orbit coupling states involved, favoring channel (viii) (Fig. 1).[23] Power dependence studies of the H^+ and H^iCl^+ ($i=35$ and/or 37) ion intensities are found to support the major photorupture mechanisms proposed. Most probably, due to partial saturation effects in the excitation process, corresponding measurements of Cl^+ ion signals are not as easily interpretable, in agreement with earlier observations.[22,30]

ACKNOWLEDGMENTS

The financial support of the University Research Fund, University of Iceland, and the Icelandic Science Foundation is gratefully acknowledged. Á.K. thanks Professor Jan Petter Hansen for his support during his stay at the physics department, University of Bergen. We also thank Þórey Anna Grétarsdóttir and Arnar Hafliðason for useful help with the project.

[1] W. C. Price, Proc. R. Soc. London, Ser. A **167**, 216 (1938).
[2] S. G. Tilford, M. L. Ginter, and J. T. Vanderslice, J. Mol. Spectrosc. **33**, 505 (1970).
[3] S. G. Tilford and M. L. Ginter, J. Mol. Spectrosc. **40**, 568 (1971).
[4] D. S. Ginter and M. L. Ginter, J. Mol. Spectrosc. **90**, 177 (1981).
[5] J. B. Nee, M. Suto, and L. C. Lee, J. Chem. Phys. **85**, 719 (1986).
[6] T. A. Spiglanin, D. W. Chandler, and D. H. Parker, Chem. Phys. Lett. **137**, 414 (1987); E. de Beer, B. G. Koenders, M. P. Koopmans, and C. A.de Lange, J. Chem. Soc., Faraday Trans. **86**, 2035 (1990); E. de Beer, W. J. Buma, and C. A. de Lange, J. Chem. Phys. **99**, 3252 (1993); H. Wang and Á. Kvaran, J. Mol. Struct. **563–564**, 235 (2001).
[7] D. S. Green, G. A. Bickel, and S. C. Wallace, J. Mol. Spectrosc. **150**, 303 (1991).
[8] D. S. Green, G. A. Bickel, and S. C. Wallace, J. Mol. Spectrosc. **150**, 354 (1991); D. S. Green and S. C. Wallace, J. Chem. Phys. **96**, 5857 (1992); Á. Kvaran, H. Wang, and Á. Logadóttir, Recent Res. Dev. Physical Chem. **2**, 233 (1998).
[9] D. S. Green, G. A. Bickel, and S. C. Wallace, J. Mol. Spectrosc. **150**, 388 (1991).
[10] Y. Xie, P. T. A. Reilly, S. Chilukuri, and R. J. Gordon, J. Chem. Phys. **95**, 854 (1991).
[11] Á. Kvaran, Á. Logadóttir, and H. Wang, J. Chem. Phys. **109**, 5856 (1998).
[12] Á. Kvaran, H. Wang, and Á. Logadóttir, J. Chem. Phys. **112**, 10811 (2000).
[13] Á. Kvaran, H. Wang, and B. G. Waage, Can. J. Phys. **79**, 197 (2001).
[14] Á. Kvaran and H. Wang, Mol. Phys. **100**, 3513 (2002).
[15] Á. Kvaran and H. Wang, J. Mol. Spectrosc. **228**, 143 (2004).
[16] R. Liyanage, R. J. Gordon, and R. W. Field, J. Chem. Phys. **109**, 8374 (1998).
[17] M. Bettendorff, S. D. Peyerimhoff, and R. J. Buenker, Chem. Phys. **66**, 261 (1982).
[18] C. Romanescu and H. P. Loock, J. Chem. Phys. **127**, 124304 (2007).
[19] C. Romanescu, S. Manzhos, D. Boldovsky, J. Clarke, and H. Loock, J. Chem. Phys. **120**, 767 (2004).
[20] A. I. Chichinin, C. Maul, and K. H. Gericke, J. Chem. Phys. **124**, 224324 (2006).
[21] A. I. Chichinin, P. S. Shternin, N. Godecke, S. Kauczok, C. Maul, O. S. Vasyutinskii, and K. H. Gericke, J. Chem. Phys. **125**, 034310 (2006).
[22] Á. Kvaran, K. Matthíasson, H. Wang, A. Bodi, and E. Jonsson, J. Chem. Phys. **129**, 164313 (2008).
[23] M. H. Alexander, X. N. Li, R. Liyanage, and R. J. Gordon, Chem. Phys. **231**, 331 (1998).
[24] K. Matthíasson, H. Wang, and Á. Kvaran, J. Mol. Spectrosc. **255**, 1 (2009).
[25] Á. Kvaran, K. Matthíasson, and H. Wang, Physical Chemistry; An Indian Journal. **1**, 11 (2006); Á. Kvaran, Ó. F. Sigurbjörnsson, and H. Wang, J. Mol. Struct. **790**, 27 (2006).
[26] G. Herzberg, *Molecular Spectra and Molecular Structure; I. Spectra of Diatomic Molecules*, 2nd ed. (Van Nostrand Reinhold, New York, 1950).
[27] H. Lefebvre-Brion and R. W. Field, *Perturbations in the Spectra of Diatomic Molecules* (Academic, London, 1986).
[28] Y. Ralchenko, A. Kramida, J. Reader, and N. A. Team, National Institute of Standards and Technology, Gaithersburg, MD, 2008.
[29] R. G. Bray and R. M. Hochstrasser, Mol. Phys. **31**, 1199 (1976); J. B. Halpern, H. Zacharias, and R. Wallenstein, J. Mol. Spectrosc. **79**, 1 (1980).
[30] H. M. Lambert, P. J. Dagdigian, and M. H. Alexander, J. Chem. Phys. **108**, 4460 (1998).